*Nxnl*2 splicing results in dual functions in neuronal cell survival and maintenance of cell integrity

Céline Jaillard[123], Aurélie Mouret[4,5], Marie-Laure Niepon[123], Emmanuelle Clérin[123], Ying Yang[123], Irene Lee-Rivera[123], , Najate Aït-Ali[123], Géraldine Millet-Puel[123], Thérèse Cronin[6], Tina Sedmak[7], Wolfgang Raffelsberger[8], Bernd Kinzel[9], Alain Trembleau[10], Olivier Poch[8], Jean Bennett[6], Uwe Wolfrum[7], Pierre-Marie Lledo[4,5], José-Alain Sahel[123*], Thierry Léveillard[123,*]

[1]Institut de la vision, INSERM, U968, Paris, F-75012, France; [2]UPMC Université Paris 06, UMR-S 968, Institut de la Vision, Paris, F-75012, France; [3]CNRS, UMR_7210, Paris, F-75012, France; [4]Institut Pasteur, F-75015 Paris, France; [5]CNRS URA2182, F-75015 Paris, France ; [6]Scheie Eye Institute, University of Pennsylvania, USA; [7]Johannes Gutenberg University of Mainz, Institute of Zoology, Cell and Matrix Biology, Muellerweg 6, D-55099 Mainz, Germany; [8]Laboratoire de Bioinformatique et Génomique Intégratives, IGBMC, Illkirch, France; [9]Novartis Pharma, Basel, Switzerland; [10]Université Pierre et Marie Curie, UMR 7102, CNRS, F-75005 Paris, France

*To whom correspondence should be addressed at: Institut de la vision, INSERM, U968, UPMC Université Paris 06, UMR-S 968, CNRS, UMR 7210, Paris, F-75012, France.

Tel: +33 153462548; Fax: +33 153462502.

Email: Thierry.leveillard@inserm.fr – J-sahel@quinze-vingts.fr

Abstract

The Rod-derived Cone Viability Factors, RdCVF and RdCVF2, have potential therapeutical interests for the treatment of inherited photoreceptor degenerations. In the mouse lacking *Nxnl2*, the gene encoding RdCVF2, the progressive decline of the visual performance of the cones in parallel with their degeneration arises due to loss of trophic support from RdCVF2. Contrarily, the progressive loss of rod visual function of the *Nxnl2-/-* mouse results from a decrease in outer segment length, mediated by a cell-autonomous mechanism involving the putative thioredoxin protein RdCVF2L, the second spliced product of the *Nxnl*2 gene. This novel signaling mechanism extends to olfaction as shown by the progressive impairment of olfaction in aged *Nxnl*2-/- mice and the protection of olfactory neurons by RdCVF2. This study shows that *Nxnl*2 is a bi-functional gene involved in the maintenance of both the function and the viability of sensory neurons.

Introduction

Inherited retinal degenerations (IRD) constitute a group of genetically heterogeneous diseases that are generally untreatable and commonly lead to blindness. The most common form of IRD, retinitis pigmentosa (RP), is characterized clinically by an initial loss of night vision resulting from the dysfunction and death of rod photoreceptors, followed by a progressive non cell-autonomous loss of cones. Through the investigation of medical approaches to prevent secondary cone death in RP patients, we have demonstrated that rods secrete trophic factors essential for cone viability, and set about identifying such factors by high content screening for trophic support of cone-enriched primary cultures (1-3). From this screen Rod-derived Cone Viability Factor (RdCVF), one of the products of the Nucleoredoxin-like 1 (*Nxnl*1) gene was isolated. Injection of RdCVF protein protects the cones of two rodent models of RP, the *rd1* mouse and the Pro23His rat (4).

In silico, we have identified a paralogue gene *Nxnl*2 that shares most of the characteristics of the gene encoding RdCVF. *Nxnl*2, like *Nxnl*1, encodes for a short isoform (respectively RdCVF2 and RdCVF) and shows similar trophic effects on cone photoreceptors (5, 6). These trophic molecules are produced by the absence of splicing of the intron in between the two coding exons and of a stop codon in frame of the first exon. The splicing of this intron leads to the production of long isoforms (RdCVF2L and RdCVFL) that possess an entire thioredoxin fold (7), unlike the short isoforms. This novel signaling pathway, involving bi-functional thioredoxin-like genes, is suggested by the finding that *Nxnl*2 expression is not restricted to the retina (5), to be further implicated in neurodegenerative diseases outside the eye. We confirm the importance of *Nxnl*2 in maintaining cone photoreceptors throughout the life of the animal by showing a gradual loss of cones preceded by loss of their function in the *Nxnl*2-/- mice. Delivering the trophic factor RdCVF2 by an AAV vector to these mice

prevented the loss of cone function. The rod function was also affected in the *Nxnl*2-/- retina as characterized by shortening of rod outer segments. In this case, treating these mice with a vector expressing the alternative *Nxnl*2 splice form, AAV-RdCVF2L, prevented this shortening. Interestingly, the messengers for RdCVF2 and RdCVF2L were also detected in olfactory neurons, and olfactory function was impaired in *Nxnl*2-/- aged mice. Taken together, these observations demonstrate that this novel signaling mechanism involving the non cell autonomous effects of RdCVF2 and the cell autonomous effects of the second *Nxnl*2 isoform RdCVF2L, supports two essential sensory systems: the retinal photoreceptor function and the non-retinal olfactory function.

Results

Construction of *Nxnl2*-/- mouse strain

Conditional gene targeting was used to create by homologous recombination an embryonic stem (ES) cell line with an allele where loxP sites frame exon 1 of the *Nxnl*2 gene (Fig. 1A). Positive-negative selection was used to enrich for the ES cells that were shown by Southern blot analysis to carry the targeted allele (Fig. 1B). The cells were injected into blastocysts and subsequently injected into foster mothers to generate chimeric mice on the non-pigmented BALB/c background. Male chimeric mice were crossed with females of a BALB/c Cre-deletor strain in which Cre recombinase is expressed exclusively in the oocytes. Heterozygote *Nxnl*2+/- mice were thus generated and confirmed by genomic PCR to be heterozygous by germ-line transmission of the recombinated allele (Fig. 1C). From sib-mating of these heterozygous mice the control wild-type (WT) and the homozygous knockout (KO) mice were produced. The genotype of litters from the mature colony used in these experiments was verified by PCR.

RdCVF2 is essential for long-term maintenance of photoreceptors

The postnatal development of retinal photoreceptors in the *Nxnl2*-/- mice aged 2 months was indistinguishable from that of controls as judged by histology and electroretinograms (ERG) (Fig. 2A, Fig. S1A, B and C). However, at 10 months of age, signs of cone photoreceptor dysfunction emerged in the mutant retinas. Photopic ERG declined as recorded by the 66% reduction of the *b*-wave amplitude as compared to control (Fig. 2A and B, Table S1). Since secreted RdCVF2 is able to prevent the death of cones *in vitro* (5), we envisaged the possibility of preventing the deficit in cone function of the *Nxnl2*-/- mouse observed at 10 months of age by AAV-mediated gene transfer of RdCVF2 of the retinal pigmented epithelium (RPE). It has been shown that subretinal injection of AAV2/6 leads to exclusive RPE transduction (8). We injected subretinally a group of 6 month-old mice with AAV2/6-RdCVF2 in one eye and another group with AAV2/6-EGFP. A third group of mice was not injected. The functional rescue was evaluated 4 months later (i.e., at 10 months of age) using ERG recording. At 10 months of age, photopic ERG shows dramatic decrease *b*-wave in untreated (53 ± 13 µV) or treated mice with AAV-GFP (59 ± 13 µV), in agreement with Figure 1A (Fig. 2C). By contrast, *Nxnl2*-/- mice treated with AAV-RdCVF2 have higher ERG amplitude (135 ± 32 µV) at 10 months. These results show that the short trophic isoform encoded by the *Nxnl2* gene is sufficient to prevent the loss of function brought into play by cone photoreceptors.

In order to investigate possible deficit in cone survival, we stained cones using the lectin Peanut Agglutinin (PNA) (6, 9). At 2 months of age, no deficit in cone density was observed for the *Nxnl2*-/- mouse retina, in agreement with the absence of cone dysfunction. However, by 10 months of age, the cone density was reduced by 23% in the *Nxnl2*-/- retina (Fig. 2D). Furthemore, in accordance to previous results (10), we observed decrease in S-cones density in *Nxnl2*-/- flat mounted retina in the ventral part of the retina. We also notice specifically in

the *Nxnl2-/-* retina, the presence of cones labeled with PNA, a marker of the cone extracellular matrix sheet, without expression of S-opsin in the ventral retina (Fig. 2E). This observation indicates that the loss of cone outer segments may precede their degeneration. Analysis of the ventral region showed that M-cones are affected to the same extend in the *Nxnl2-/-* retina (Fig. 2F). This result suggests that cone photoreceptors were undergoing progressive degeneration preceded by functional loss, supporting the fact that *Nxnl2* encodes for a cone viability factor, RdCVF2, involved in the maintenance of cones in the adult animal. It should be noted that the degeneration of cones was observed in the presence of the potentially compensating gene *Nxnl1* gene.

Absence of RdCVF2L induces shortening of the outer segment length

Since both RdCVF2 and RdCVF2L are expressed by rods (5), we also evaluated rod function of the *Nxnl2-/-* mouse. A decrease in the *Nxnl*2-/- *a*-wave amplitudes in mice aged 10 months was shown to increase with light intensity (Fig. 3A and B and Table S1). However, the reduction in rod function does not result from a reduced rod viability since the outer nuclear layer (ONL) compose of 97% rods is not decreased in aged *Nxnl2-/-* mice compared to controls (Fig. 3C and D). We decided to explore cone morphology in *Nxnl2+/+* and *Nxnl2-/-* retina mice. Whereas a disruption of outer segment of *Nxnl1-/-* mice was shown using tomography electron microscopy, no extracellular space between segmented stacks was observed in rod outer segment of *Nxnl2- /-* mice at 12 months of age (Fig. 4 A-C). However, scanning electron microscopy revealed a decreased in length of *Nnll2-/-* outer segment compared to control (8.7 ± 1.2 µm vs 12 ± 1.3 µm) (Fig. 4D and E). Then, we envisaged an alternative cause for dysfunction of rods and considered a possible reduction in the outer segments. To address this directly, we isolated the photoreceptor sensory cilium (PSC) complexes from wild-type and *Nxnl2-/-* mouse retinas (11). The isolated PSC complexes stained with anti-rhodopsin and anti-RPGRIP antibodies, both expressed by rods, consist

essentially of rod-photoreceptor outer segments (Fig. 4F). At 3 months of age, there is no difference in length of outer segment between *Nxnl*2+/+ and *Nxnl*2-/- retina mice (Fig. 4H). However, we observed a decrease of outer segment length in *Nxnl*2-/- compared to *Nxnl*2+/+ at 10 months (8.36 ± 0.35 µm vs 10.57 ± 0.24µm) (Fig. 4G and H). The rod outer segments were purified used laser capture microdissection by cutting them as indicated (Fig. 4I). Western blotting analysis of these preparations showed that opsin content of the rod outer segment is reduced in the absence of the *Nxnl*2 gene (Fig. 4I left panel) whereas rhodopsin content is not affected in the whole retina (Fig. 4I, right panel).

In order to check whether RdCVF2L is implicated in the maintenance of the outer segment, we injected subretinally a group of 7 month-old *Nxnl*2-/- mice with AAV2/8-RdCVF2L or AAV2/8-EGFP. The AAV2/8 serotype was chosen as it efficiently achieves expression within photoreceptor cells. Mice were sacrificed 3 months later in same period of the light cycle and the presence of GFP fluorescence in the photoreceptor layer in the AAV-GFP injected animals was confirmed (Fig. 4J). The length of outer segment of *Nxnl*2-/- injected with AAV-GFP was no significantly different from that of non-injected *Nxnl*2-/- mice (7.88 ± 0.40 µm vs 8.36 ± 0.35µm) (Fig. 4K). However, retina injected with AAV-RdCVF2L exhibit longer outer segment (12.58 ± 0.81 µm vs 7.88 ± 0.40 µm). These results demonstrate that one of the products of the *Nxnl*2 gene, the thioredoxin protein RdCVF2L, is involved in maintenance of outer segment.

The inactivation of *Nxnl2* induced stress, TAU hyperphosphorylation and down-regulation of the Wnt pathway

Microarray profiling of retinal RNA from wild-type and *Nxnl*2-/- mice at post-natal day 40 (PN40) was performed to identify molecular events implicated in the *Nxnl*2 signaling pathway (12). The largest significant fold change apart from *Nxnl*2 itself was observed for Endothelin

2 (Edn2) which is increased 43-fold in the *Nxnl*2-/- retinas as compared to controls (Table S2, http://lbgi.igbmc.fr/Nxnl2/). We have previously reported Edn2 induction, (same probeset 1449161_at) in the *Nxnl*1-/- retinas at PN40, a marker of stress induced in most models of photoreceptor disease or injury (6, 13). Cumulative stress in the *Nxnl*2-/- retina is also evidenced by the increased expression of glial fibrillary acidic protein (GFAP) from 7 to 18 months (Fig. 5A and Fig. S1A, B and C). We also observed that the probesets for the transcription factor Sox30 (1440509_at) and Transgelin 2 (Tagln2, 1439407_x_at) that encodes for a protein involved in the organization and dynamics of the actin cytoskeleton are upregulated in both *Nxnl*2-/- and *Nxnl*1-/- retinas (Table S2). They may represent markers of the stress generated by a deficit in RdCVF signaling, that may cause the activation of microglial cells in the retina (6, 12). Interestingly, transgelin was shown to be overexpressed in the brains of patients affected by Alzheimer's disease (14), a fact that may be related to the observation that the microtubule associated protein TAU is hyperphosphorylated and aggregated in the retina of the *Nxnl*1-/- mouse, a model with progressive rod loss (6, 15). We therefore analyzed the status of TAU phosphorylation using AT8 antibody in 10 month-old *Nxnl*2-/- mice. Whereas no difference was observed in the overall expression of TAU using the tau5 antibody, the *Nxnl*2-/- retina exhibits a hyperphosphorylation of TAU compared to control throughout the three different layers of the retina (Fig. 5B). Overall the comparison of markers associated with the mouse carrying an inactivation of either *Nxnl*1 or *Nxnl*2 does not account for the lack of rod cell death in the *Nxnl*2 retina when compared to the *Nxnl*1 retina. However, the genes whose expression is shown by the microarray data to be reduced in the *Nxnl*2-/- retina may offer mechanistic insights into RdCVF2's role in the retina. Among these, are genes involved in the Wnt signaling pathway: secreted frizzled-related protein 1 (Sfrp1, 1428136_at) and the homologue of beta-catenin, armadillo repeat containing 9 (Armc9, 1454213_at, Fig. 5D) which are down-regulated by 2.3 and 4-fold respectively. The analysis

of *Nxnl*2-/- retinal lysates by western blotting confirms that beta-catenin is downregulated (Fig. 5C), indicating a possible resemblance with the nucleoredoxin pathway (16). We also noticed that the expression of *Nxnl*2 is reduced in the *Nxnl*1-/- retina (Fig. 5D). The expression of *Nxnl1* is slightly increased in the retina of the *Nxnl2-/-* mouse (data not shown).

*Nxnl*2 is expressed by olfactory sensory neurons

We have previously reported that in addition to being expressed by the photoreceptors of the retina, *Nxnl*2 is also expressed in the brain (5). The transcriptomic data available in the SymAtlas database (http://biogps.gnf.org), reveals *Nxnl*2 (gnf1m10508_a_at) to be expressed at several orders of magnitude higher in the retina and the olfactory epithelium over the 78 other mouse tissues examined. To localize the expression of *Nxnl*2 in the olfactory epithelium, we performed in situ hybridization with riboprobes specific for the two alternative mRNAs encoding RdCVF2 and RdCVF2L. In situ hybridization revealed that RdCVF2 and RdCVF2L mRNAs are expressed throughout the olfactory sensory neurons (OSN) layer of the nasal epithelium (Fig. 6A-D). After bulbectomy treatment (OBX) (17, 18), expressions of both RdCVF2 and RdCVF2L mRNAs were found to be sharply decreased establishing that both isoforms are expressed by olfactory neurons (Fig. 6E and F).

Impaired olfactory discrimination of the *Nxnl2-/-* mice with age

The expression of *Nxnl2* by olfactory neurons indicates a possible implication of this gene in the maintenance of the olfactory function in the adult mouse, paralleling its functional impact on vision. To explore olfactory function of the *Nxnl2-/-* mouse, we performed olfactory discrimination learning tests. We trained *Nxnl2-/-* mice and controls with an odor pair (two enantiomers) using a go/no-go olfactory conditioning task (Fig. 7A). In this paradigm, water-deprived mice are trained to discriminate between a water-rewarded odorant stimulus [odor S+, (+)-Carvone] and an non-rewarded odorant stimulus [odor S−, (-)-Carvone]. Mice are

rewarded with water for licking in response to odor S+ while correct withholding of licking to odor S- is not rewarded. *Nxnl2-/-* and control mice reached a learning criterion (set to 85% of correct responses), on average within 400 trials (Fig. 7B). This procedure showed that both young (2 months) and old (12 months) *Nxnl2-/-* mice were able to detect the odors present in both solutions. This eliminated any problem in gross olfactory sensitivity. We noticed that the training of 12-month-old *Nxnl2-/-* mice was more tedious, although the test was not sensitive enough to identify any difference in olfactory discrimination ability. To increase the sensitivity of the task, we then trained mice to discriminate between two binary mixtures of carvone enantiomers. Over training sessions, the two mixtures became progressively more similar, which increased the task difficulty. For 2-month-old mice, correct responses were similar between *Nxnl2-/-* and control mice for each mixture of (+)-Carvone and (-)-Carvone used (from easy to difficult tasks) (Fig. 7C). This result is also shown in the mean percentage of correct responses with each mixture (Fig. 7D). In sharp contrast with these observations, at 12 months of age, we observed a decline in the ability of mice to perform fine odor discrimination, independently of the genotype. These results are in agreement with another study, showing a progressive reduction of mice fine olfactory discrimination performance with aging (19). When exposed to a 99/1 mixture, old wild-type mice failed to perform the task correctly, whereas young animals were still able to discriminate both solutions (Fig. 7C). Interestingly, the performance of, *Nxnl2-/-* mice was worse, since they already failed to reach the performance criterion with the 98/2 mixture (Fig. 7C). The difference in discrimination responses between *Nxnl2-/-* and control mice became significant for the 80/20 mixture (Fig. 7D). Taken together, these results show that the *Nxnl2-/-* mice present a stronger age-dependent impairment of fine odor discrimination.

RdCVF2 promotes survival of olfactory sensory neurons in vitro

The reported trophic activity of RdCVF2 on cultured cone photoreceptors (5), suggested that the age-dependant impairment of odor discrimination of the *Nxnl2*-/- mouse may result, at least in part, from a dysfunction resulting from the absence of trophic support to OSNs. However, it should be noted that in contrast to photoreceptors, OSNs regenerate throughout the life of the animal thus compensating for any gradual loss of neurons (20). We nevertheless evaluated the trophic activity of the two products of the *Nxnl2* gene, RdCVF2 and RdCVF2L, on adult cultures of β-tubulin III positive OSNs. Primary cultures of purified adult OSN were performed according to a previous report (21). These authors have shown that after one day of culture, two main cell populations are found in cultures: OSNs and epithelioid cells, including supporting and basal cells. After five days in vitro, neurons died and only supporting and basal cells survived. We prepared OSN cultures from a wild-type mouse (BALB/c) and incubated them for five days in the presence of conditioned media from COS-1 cells transfected with the empty vector pcDNA3, or alternatively with pcDNA-RdCVF2 or pcDNA-RdCVF2L. The number of surviving β-tubulin III positive cells is higher with cells transfected with RdCVF2 or RdCVF2-L than in controls (Fig. 8A-C). We also tested the survival activity toward OSNs of purified RdCVF2 and RdCVF2L as a fusion protein with gluthatione-S-transferase (GST). The addition of GST-RdCVF2 and GST-RdCVF2L resulted in a significant increase in the number of OSNs as compared to GST (Fig. 8D). Since this effect may reflect an enhanced differentiation of epithelioid cells to olfactory neurons in the presence of RdCVF2 proteins, cultures were established in serum free medium without any growth factor for 5 days in vitro (at this time, no more OSNs survived, only basal cells survived) and RdCVF2 was added for 3 days. Differentiation was no significant increase in β-tubulin III-positive cells in cultures treated with GST-RdCVF2 or GST-RdCVF2-L compared with GST showing no differentiation of basal cells into neurons. These results demonstrate

the existence of a trophic effect directed specifically to OSNs. Notably, this trophic effect was more pronounced for the short trophic isoform RdCVF2, the truncated thioredoxin-like protein.

Discussion

The *Nxnl2* gene was originally identified through its homology with *Nxnl1*, the gene encoding the trophic factor RdCVF. The therapeutic potential of this latter gene is being investigated for patients suffering from retinitis pigmentosa, an inherited retinal disease characterized by the sequential loss of rod and cone photoreceptors (2). The short isoforms of the nucleoredoxin-like genes, the RdCVF and RdCVF2 proteins are *bona fide* trophic factors whose action is relayed by the activation of an as yet unidentified cell surface receptor that mediates a cascade of events leading to the survival of the target cells. Within the thioredoxin family the short RdCVF proteins are comparable to TRX80, the truncated product of TRX1, which acts as a cytokine of the immune system and does not require the cysteines of the thioredoxin catalytic site (22). It is possible that RdCVF and RdCVF2, prevent the death of cones by maintaining their functionality, and indirectly activating a survival pathway. We observed here that the decrease in function of the cones of the *Nxnl2-/-* mouse is of higher amplitude than the actual cone cell loss and consequently the impairment in function precedes the cell death (Fig. 1A-C). We also showed that the short RdCVF2 protein when delivered into the retina by an AAV vector, achieves almost complete rescue of cone photoreceptor function of the *Nxnl2-/-* mouse. This demonstrates that the cone dysfunction arises in this model due to lack of trophic support from the short protein RdCVF2.

We consider the possibility that the production of the RdCVF trophic factors is a result of fortuitous inhibition of splicing of an ancestral thioredoxin gene. The resulting genes would be bi-functional with one secreted product aimed at protecting the cones and another product,

an active thioredoxin involved in an unrelated process. In this regard, it is worth remembering that retinal diseases are part of the group commonly termed neurodegenerations, for which a wealth of studies have highlighted the role of oxidative stress as a causative or accelerating factor. Oxidative stress may trigger an RdCVF-based redox signaling detected by the long isoforms produced by splicing of the two exons of the nucleoredoxin-like genes: RdCVFL and RdCVF2L. We have formulated the hypothesis that both isoforms of these genes participate in the same signaling pathway, in which the long isoform, an enzyme, would be sensor of the oxidative stress coordinating an adaptive trophic response from the short isoform (2). However thiol-oxydoreductase activity has not been directly demonstrated for these proteins. Instead the recently identified protein-protein interaction between RdCVFL and TAU may serve as an indirect measure of oxidative stress and hence as the environmental cue for a trophic response. This interaction has led us to demonstrate hyperphosphorylation of TAU in the *Nxnl1-/-* (15), and now in the *Nxnl2-/-* retinas. Furthermore, RdCVFL was shown to inhibit TAU phosphorylation *in vitro* and to prevent its degradation by oxidation. Our interpretation of these results is that the RdCVFL protein exerts a cell-autonomous function within the rod photoreceptors, which in its absence causes a rod degeneration accompanied by TAU aggregation (12). This long isoform encoded by the *Nxnl1* gene may thus be involved in the defense of rod photoreceptors against photo-oxidative stress. Interestingly, the main difference in the visual phenotype of the *Nxnl2-/-* mouse as compared to the *Nxnl1-/-* mouse is the absence of thinning of the outer nuclear layer in the *Nxnl2-/-* retina, a cellular layer composed of 97% rods (Fig. 2 C-D). Both mouse models exhibit a dysfunction of rod photoreceptors but only the *Nxnl1-/-* shows a progressive loss of rod cells whereas *Nxnl2-/-* exhibit a defect in rhodopsin transport. We have examined the transcriptome of the retina of the *Nxnl2-/-* at PN40, before the loss of function starts and compared it to that of the *Nxnl1-/-* under the same conditions. We could not find any striking differences that could explain the

lack of death of the rods in the absence of *Nxnl2*. The transcriptomes of both mouse models display sign of injury response and microglial activation.

When the RdCVF2L and RdCVFL protein sequences are compared the most striking difference is the absence of conservation of the most C-terminal cysteine of the catalytic site of thioredoxin in RdCVF2L. This cysteine has been replaced by a serine residue in the mammalian *Nxnl2* genes (5). Without this critical cysteine residue, it is unlikely that RdCVF2L would have a thiol-oxydoreductase activity toward protein substrates, and consequently would not participate directly in a direct defense mechanisms against oxidative stress (23). Given these considerations we looked at alternatives that may explain the dysfunction of rod photoreceptors in the *Nxnl2-/-* mouse. We detected a reduction in the length of rod outer segments. We demonstrated that the deficit can be reverted by reintroducing the RdCVF2L protein using an AAV vector. The mislocalization of rhodopsin in the cell bodies of the ONL and microtubule disorganization have been described in other forms of murine retinal degeneration such as in mice lacking *Rp1*, *Bbs2* and *Bbs4* or *myosin 7A* genes (24-27). In these models, protein transport is impaired. In addition, *Bbs1-/-* and *Bbs4-/-* mice have deficits in smell which resemble the olfactory deficit reported here in *Nxnl2-/-* mouse (28). Therefore, the *Nxnl2* gene encoding for a short RdCVF2 protein is necessary for neuronal survival while the long isoform, RdCVF2L may act in the transport of rhodopsin protein to the outer segments of rod cells. Understanding the mechanism by which RdCVF2L is participating in the maintenance of outer segment length will require further investigation, and may involve its interaction with the Wnt/beta-catenin pathway (16). It is also known that thiorexdoxin proteins have chaperone activity that does not rely on the catalytic site (29).

We have further demonstrated that RdCVF signaling extends to other sensory organs in addition to the eye. Expression of the *Nxnl2* gene was observed in the olfactory epithelium

(Fig. 6) and more specifically by OSNs. It is presently unknown whether distinct sub-types of OSNs exist corresponding to the two classes of photoreceptors, the rods and the cones. However some differences clearly exist within these cells as different OSNs express distinct classes of G-protein coupled receptors, the well-characterized protein superfamily that includes opsins (30). Some of these sensory neurons can be protected *in vitro* by RdCVF2, and to a lesser extent by RdCVF2L (Fig. 8). A role of the *Nxnl2* gene in maintaining the function of the OSN neurons throughout life is supported by the deficit in olfactory discrimination in the aged *Nxnl2-/-* mice (Fig. 7). Here again, as for the cone function, the phenotype is linked to the age of the animal. It is possible the *Nxnl2-/-* mouse represents a model of accelerated aging of sensory systems. Since OSNs regenerate throughout life, their increased death in the absence of the protection by the trophic factor RdCVF2 would finally, at a late age, saturate the regenerative process leading to the observed dysfunction. Alternatively, and based on a possible deficit in rhodopsin transport to the outer segments and on the fact that TAU is found to be hyperphosphorylated in olfactory epithelium (Fig. S2), the dysfunction in olfactory discrimination may result from a progressive defect in the transport of odorant receptor molecules throughout the cilium of these neurons. It remains to characterize what molecular mechanisms in aging create such conditions.

We have described here the phenotype of the mouse lacking the *Nxnl2* gene, the paralogue of the *Nxnl1* gene that encodes the therapeutic RdCVF protein. Our results show that *Nxnl1* and *Nxnl2* belong to two distinct signaling pathways, though they may possibly interact as shown by the reduction of the expression of *Nxnl2* in the *Nxnl1-/-* retina (Fig. 5D). The bi-functional nature of these genes encoding two protein products participating in a coordinated action is demonstrated here by the deficit in the maintenance of outer segments attributed to RdCVF2L. The extension of this novel signaling to the olfactory system opens the possibility

that it extends more broadly in the nervous system and may be involved in a range of neurodegenerative diseases that includes but is not restricted to inherited retinal degeneration.

Materials and methods

Animals. Experiments were conducted in accordance with the ARVO Statement for the Use of Animals in Ophthalmic and Vision Research and with protocols approved by the National Eye Institute Animal Care and Use Committee. Animals were housed under a 12 hours light/12 hours dark cycle and given *ad-libitum* access to food and water.

Generation of *Nxnl*2 Knockout Mice. *Nxnl*2 genomic sequences corresponding to *Nxnl*2 5'UTR, exon 1 and intron 1 were amplified from BALB/c mouse genomic DNA and subcloned into a modified targeting vector containing a loxP element and an FRT flanked neomycin cassette. Subcloned sequences were compared to sequences available from the Mouse Ensembl database (gene ID: ENSMUSG00000021396). Finally, a loxP element was inserted into the 5'UTR upstream of exon 1, resulting in the plasmid p*Nxnl*2 target. BALB/c mouse ES cell culture was performed with primary X-ray-inactivated embryonic fibroblasts derived from DR4 mice. ES cells were transfected by electroporation using 12 μg of linearized p*Nxnl*2 target. Transfected ES cells were selected for neomycin resistance using 0.2 mg/ml geneticin (Invitrogen). Ten days after transfection, G418-resistant ES cell clones were isolated and analyzed by polymerase chain reaction (PCR) for homologous recombination as well as for the presence of the loxP element integrated into the *Nxnl*2 5'UTR. To remove the neomycin selection cassette targeted ES cells were transfected with an Flpe expression plasmid. Individual ES cell clones were subsequently screened for neomycin sensitivity. DNA was prepared from selected neomycin-sensitive ES cell clones and analyzed by PCR for the loss of the selection cassette. Southern blotting was performed on 12 μg of genomic DNA,

digested with 30 units of the XbaI as above. Southern blotting was performed on 12 μg of genomic DNA, digested with 30 units of the HindIII or MunI/Asp718 restriction enzymes and separated on a 1% agarose gel. After denaturation the DNA was blotted on a Hybond N+ membrane (GE Healthcare) followed by UV crosslinking. Hybridization with the ^{32}P-labeled DNA probe (Rediprime II Random prime labeling kit, GE Healthcare) was performed in Perfect Plus Hybridization buffer (Sigma) at 65°C overnight. After washing of the hybridized membrane, image analysis was performed using a phosphoimager. Targeted BALB/c ES cells were injected into C57Bl/6 host blastocysts, which were then transferred into pseudopregnant CB6F1 foster mothers. Chimeric offspring were identified by coat pigmentation (white BALB/c on a black C57Bl/6 background). White offspring indicated the germline transmission of the targeted ES cells and were further analyzed for their correct genotype. In order to generate *Nxnl*2 knock-out mice, targeted mice were mated with BALB/c Cre deleter females [C-TgN(CMV-Cre)#Cgn] (31), resulting in Cre mediated loxP recombination and the excision of the floxed exon 1. Offspring were analyzed for their genotype by PCR, performed on genomic DNA prepared from tail biopsies using following primers: P1: 5'-TCCTATATGCTGGTTTCCGTC-3'; P2: 5'-TGATCAAGGAGCCTAGCTAAGG-3'; P3: 5'-TCGATTAGAGGTAGAAGAACCC-3' and P4: 5'-AGCTCCGTGTAGAAGTCGC-3'.

Cone counting. Cone counting in whole retina was performed on mice at 10 months of age according to the protocol described previously (6). Briefly, retina were dissected, fixed and labeled with the lectin Peanut Agglutinin (PNA) (1/40) and Opsin (1/250) (9) (10). Counting was performed on automatic platform (10).

Immunohistochemistry. Mouse eyes were fixed by immersion in 4% paraformaldehyde in PBS for 4 hours at 4°C, cryoprotected in 30% sucrose, and embedded in OCT. Antibodies were diluted in blocking buffer (5% BSA in PBS-Tween 0.05%), at dilutions of 1/250 for the

rhodopsin antibody (Rho-4D2, gift from David Hicks, Strasbourg, France), 1/1000 for

recoverin (Millipore, MA, USA) Q2, RPE65 (Abcam, Cambridge, UK), GFAP (Dako,

Glostrup, Denmark) and glutamine synthetase (Chemicon, Millipore, MA, USA). A

concentration of 1/100 for RPGRIP (generous gift from Aziz El Amraoui, Paris, France).

Primary antibodies were detected with Alexa 488 or Alexa 594 conjugated goat anti-mouse or

goat anti-rabbit antibodies.

In situ **hybridization**. The expression of RdCVF2 and RdCVF2L mRNA in the olfactory

epithelium was analyzed by *in situ* hybridization with a digoxigenin-labeled murine antisense

riboprobe. After defrosting and drying at room temperature, sections were post-fixed on ice

for 10 min in 4% paraformaldehyde and washed in PBS at room temperature for 10 min.

Sections were hybridized with sense and antisense RdCVF2 and RdCVF2L riboprobes

generated from SP6 or T7 promoters and labeled with digoxigenin-UTP (Boehringer,

Mannheim, Germany) as described previously (5).

Isolation of Mouse photoreceptor sensory cilium (PSC) and dissection of outer segment

Retinas were dissected and transferred to 1 ml of PBS with calcium. They were vortexed for

30 seconds. Using a wide-open pipette, PSC solution was transferred on a superfrost slide and

fixed with 1:1 methanol and acetone for 10 minutes. To isolate outer segment, slides were

mounted on a Leica micro dissection laser system DM 6000 (Leica, Germany) with the

section facing downwards. Using a 63x objective, cutting intensity, aperture and velocity were

adjusted as follows: Aperture 20, intensity 45, speed 1, offset 45. Then, the pulsed UV laser

beam was carefully directed along the borders of outer segment. Outer segments were then

transferred by gravity into a microcentrifuge tube cap placed directly underneath the section.

Western Blot Analysis. Cell lysate was homogenized by sonication in a lysis buffer containing 50 mM Tris-HCl pH 7.5, 1 mM PMSF, 1 mM EDTA, 1 mM dithiothreitol, 1% Triton X-100, protease inhibitors, 50 µg/ml TLCK, 1 mM sodium fluoride and 1 mM sodium orthovanadate. Ten µg of proteins were resolved by 12% SDS-PAGE and transferred onto nitrocellulose. The membrane was saturated with PBS, 0.05% Tween-20, 5% nonfat dry milk for 1 hour at room temperature and then incubated overnight at 4°C with antibodies. The membrane was then washed and incubated with the peroxidase-conjugated goat anti-rabbit or anti-mouse secondary antibody (1/15,000; Jackson ImmunoResearch Laboratories, Hamburg, Germany) for 1 hour. Antibody binding was detected by Enhanced Chemiluminescence system and hyperfilm-ECL X-ray film (ECL+, Amersham Pharmacia Biotech) as recommended by the manufacturer.

Microarray analysis[a]

Using purified retinal RNA from PN40 mice, cDNA probes were subsequently generated and hybridized to Affymetrix gene chips (mouse genome 430 2.0 array). Three replicates were performed for each experiment. Quality control (QC) was performed using RReportGenerator (32) and Affymetrix raw data were summarized and normalized using genehip robust multi-array analysis (gcrma) using R/Bioconductor) and filtered to remove genes with very low signal intensities in all samples as described previously (6). Testing for differential gene expression was performed i) using an empirical Bayes shrinkage (package "limma") and ii) using the fdr2d procedure (package "OCplus") (33). The final selection of probe-sets characterizing the *Nxnl2*+/+ and *Nxnl2*-/- transcriptomes was performed based on local false discovery rate (FDR) values.

---

[a] GEO Series GSE21863

Scanning electron microscopy

Mouse was fixed using paraformaldehyde 4%, glutaraldehyde 2% in cacodylate sodium buffer 0.2 M pH 7.4. Eyes were enucleated and cut in several pieces. They were incubated overnight in the perfusion solution. Then they were rinced in cacodylate sodium buffer. Eyes were post-fixed in osmium tetroxide 2% in cacodylate buffer 1 hr and rinsed in ultra pure water. Samples were dehydrated in a grade of alcohol. They were dried by critical point drying method. Samples were dried by evaporation of carbon monoxide. Then they were fixed on an aluminum support and placed in Scancoat six Edwards and metal coated with gold by spray. Observations were made using a scanning electron microscope Cambridge S260 at 10 kV under a pression of 10^{-7} torr.

Transmission electron microscopy. The eye cups were fixed in 2.5% glutharaldehyde at room temperature 2h, extensively washed overnight and post-fixed in osmium tetraoxide 1% for 1h at room temperature. Samples were washed in Ringer–Krebs Buffer (140mM NaCl; 4.5mM KCl, 2.2mM CaCl 2,12mM MgSO4, 12mM NaHCO3, 0.44mM KH2PO4, 5.55mM glucose, pH¼7.4) followed by dehydration in graded ethanol and acetone. They were embedded in epoxy resin and ultrathin sections (400 to 600nm) were cut and stained with uranyl acetate and lead citrate and observed under an electron microscope (Met Zeiss 912, at 80kV).

Semithin sectioning and outer nuclear layer (ONL) measurement. Mice (n=6) were anesthetized by a mixture of ketamine (160 mg/kg)/xylazine (32 mg/kg) followed immediately by vascular perfusion of glutharaldehyde 2.5% and formaldehyde 2% in PBS. The eyes were embedded in epoxy resin and histological sections of 1-mm thick were made along the sagital axis at the optic nerve level as previously described.38 Briefly, in each of the superior (dorsal) and inferior (ventral) hemispheres, ONL thickness was measured in nine sets

of three measurements each (total of 27 measurements in each hemisphere). Each set was centered on adjacent 250-mm lengths of the retina, with the first set centered 250 mm from the optic nerve head and subsequent sets located more peripherally. Within each 250-mm length, the three measurements were made at defined points separated from one another by 50 mm. The 54 measurements in the two hemispheres sampled are representative of the entire retina.

Generation of recombinant AAV vectors. The AAV2/6.1 vector was created by mutating a particular AAV2 capsid residue (the lysine residue at position 531 was mutated to glutamic acid), thereby ablating the heparin binding motif of the AAV2 capsid (34, 35). The modified capsid sequence was cloned into an AAV packaging construct. Both for AAV2/6.1 and AAV2/8, the AAV cis plasmid contains AAV2 inverted terminal repeats (ITRs) bordering the transgene cassette. The cassette consists of the RdCVF2, RdCVF2L or GFP cDNA driven by the CMV promoter and carrying an SV40 poly(A). Recombinant AAV was generated by triple transfection of 293 cells with the cis-plasmid, adenovirus helper plasmid and the packaging construct as described previously (36). Recombinant AAV was purified by $CsCl_2$ sedimentation, and genome copy (GC) titers of the vectors were determined by TaqMan (Applied Biosystems) analysis by using probes and primers targeting the SV40 poly(A) region.

Delivery of the AAV constructs to *Nxnl2-/-* mouse retina. Animals were anesthetized, and intraocular injections were performed with a technique similar to that described earlier by inserting a needle into the eye posterior to the limbus (4). *Nxnl2-/-* mice were injected with 1 µl of AAVRdCVF2, AAVRdCVF2L or AAVGFP at 3.10^{12} genome copies (gc/ml) into the right eye.

ERG recording. Following overnight dark adaptation, animals were prepared for recording. Under intramuscular anesthesia with a mixture of ketamine (100 mg/kg) and xylazine (10 mg/kg), pupils were dilated with 0.5% Tropicamide or 1% Atropine and the cornea was locally anesthetized with Oxbuprocaine application. Body temperature was maintained near 37°C with a heating pad. An electrode was placed on the corneal surface. A reference electrode was inserted subcutaneously on the head of the mice and a needle electrode inserted subcutaneously in the back served as ground. The light stimulus was provided by a 150 watt xenon lamp in a Ganzfeld stimulator (Multiliner Vision, Jaeger Toennies, Germany). Following overnight dark-adaptation rod responses were determined to flash intensities between 100 and 10 000 mcds/m^2. Each scotopic ERG represents the average of five responses from a set of five flashes of stimulation. To isolate cone responses a 10-min light saturation at 25 cds/m^2 was used to desensitize the rods. The cone photopic ERGs shown represents the average of 10 responses from 10 consecutive flashes at 10 cds/m^2 intensity.

Production of GST-RdCVF2 and GST-RdCVF2L

RdCVF2 and RdCVF2L were cloned into pGEX-2TK plasmid (GH Healthcare), expressed and purified as described previously (1).

Bulbectomy and real time RT-PCR. Two-month old mice were given a survival dose of anesthetic (ketamine 60 mg/kg, xylazine 20 mg/kg) by intraperitoneal injection. A rostral to caudal incision was made above the nose to behind the ears. With the skin held open, a small hole was made in the frontal bone over the right olfactory bulb using a drill and the bulb was removed by aspiration. The skin was sutured and animals were housed singly during recovery. After 6 days, animals were killed by cervical dislocation and olfactory epithelium was dissected, and the right and left sides were separated and placed in guanidine HCl buffer

(Promega). RNA was purified from a cesium chloride gradient (37). Real-time RT-PCR

(Light cycler, Roche) was performed as described previously (38) .RdCVF2 and RdCVF2L

were amplified using respectively the following primers:

5'-CCGTGCTATTGTTTCAGAGCCCTTAACTTTCTATC-3',

5'-CTGACACTCCAATCGTAA-AAGGCAGAAAACGC-3' and 5'-CATCACCAAC

AAAGGGCG GAAG-3', 5'-CATTCCTCAGCAGAGAAG GGAA C-3'.

Odor discrimination task. Mice were trained using an operant conditioning go/no-go

procedure in home-made computer-controlled olfactometers (39). In this paradigm, the

presence of the positive odor stimulus (S+) was associated with a water reward obtained by

licking a water delivery tube. For the negative odor stimulus (S−), mice received no water

reward and had to refrain from licking. In each trial, a single stimulus (S+ or S−) was

presented, and the percentage of correct responses was determined for each block of 20 trials.

All mice underwent a session of 10 blocks per day. Olfactory discrimination performances

were determined with monomolecular odor compounds and binary odor mixtures (see

Supplemental Methods).

Olfactory neuron cell culture. After removal from the nasal septum, the mouse olfactory

epithelium was separated from the underlying lamina propria and cultured (40). Briefly, the

olfactory mucosa was incubated for 45 min at 37°C in 5% CO_2 in a 2.4 U/ml dispase II

solution (Roche) until the olfactory epithelium could be carefully dissected away from the

lamina propria. The olfactory epithelium was then gently triturated to separate cells. Cells

were then plated at a density of 2,000 cells per well in a plastic 24-well tissue culture plate

(Nunc, Naperville, IL, USA), which had been coated at 5 µg/cm^2 with collagen type IV

(Sigma, St Louis, MO, USA). Cells were cultured in serum-free DMEM-ITS in the presence

of conditioned media from COS-1 cells transfected with empty vector pcDNA3, pcDNA-RdCVF2, pcDNA-RdCVF2L or GST-RdCVF2, GST-RdCVF2L or GST. Medium was changed every 48 hours. After 5 days, cells were counted after labeling with anti β-tubulin III antibody.

Conflict of interest statement

CJ, JAS and TL have a patent on *Nxnl2* for neurological diseases.

References

1   Léveillard, T., Mohand-Said, S., Lorentz, O., Hicks, D., Fintz, A.C., Clerin, E., Simonutti, M., Forster, V., Cavusoglu, N., Chalmel, F. *et al.* (2004) Identification and characterization of rod-derived cone viability factor. *Nat. Genet.*, **36**, 755-759.

2   Léveillard, T. and Sahel, J.A. (2010) Rod-derived cone viability factor for treating blinding diseases: from clinic to redox signaling. *Sci. Transl. Med.*, **2**, 26ps16.

3   Mohand-Said, S., Deudon-Combe, A., Hicks, D., Simonutti, M., Forster, V., Fintz, A.C., Leveillard, T., Dreyfus, H. and Sahel, J.A. (1998) Normal retina releases a diffusible factor stimulating cone survival in the retinal degeneration mouse. *Proc. Natl. Acad. Sci. U S A*, **95**, 8357-8362.

4   Yang, Y., Mohand-Said, S., Danan, A., Simonutti, M., Fontaine, V., Clerin, E., Picaud, S., Leveillard, T. and Sahel, J.A. (2009) Functional cone rescue by RdCVF protein in a dominant model of retinitis pigmentosa. *Mol. Ther.*, **17**, 787-795.

5   Chalmel, F., Leveillard, T., Jaillard, C., Lardenois, A., Berdugo, N., Morel, E., Koehl, P., Lambrou, G., Holmgren, A., Sahel, J.A. *et al.* (2007) Rod-derived Cone Viability Factor-2 is a novel bifunctional-thioredoxin-like protein with therapeutic potential. *BMC Mol. Biol.*, **8**, 74.

6   Cronin, T., Raffelsberger, W., Lee-Rivera, I., Jaillard, C., Niepon, M.L., Kinzel, B., Clerin, E., Petrosian, A., Picaud, S., Poch, O. *et al.* (2010) The disruption of the rod-derived cone viability gene leads to photoreceptor dysfunction and susceptibility to oxidative stress. *Cell Death Differ*.

7   Lillig, C.H. and Holmgren, A. (2007) Thioredoxin and related molecules--from biology to health and disease. *Antioxid. Redox Signal.*, **9**, 25-47.

8   Yang, G.S., Schmidt, M., Yan, Z., Lindbloom, J.D., Harding, T.C., Donahue, B.A., Engelhardt, J.F., Kotin, R. and Davidson, B.L. (2002) Virus-mediated transduction of murine retina with adeno-associated virus: effects of viral capsid and genome size. *J. Virol.*, **76**, 7651-7660.

9   Blanks, J.C. and Johnson, L.V. (1984) Specific binding of peanut lectin to a class of retinal photoreceptor cells. A species comparison. *Invest. Ophthalmol. Vis. Sci.*, **25**, 546-557.

10   Clerin, E., Wicker, N., Mohand-Said, S., Poch, O., Sahel, J.A. and Leveillard, T. (2012) e-conome: an automated tissue counting platform of cone photoreceptors for rodent models of retinitis pigmentosa. *BMC Ophthalmol.*, **11**, 38.

11   Liu, Q., Tan, G., Levenkova, N., Li, T., Pugh, E.N., Jr., Rux, J.J., Speicher, D.W. and Pierce, E.A. (2007) The proteome of the mouse photoreceptor sensory cilium complex. *Mol Cell Proteomics*, **6**, 1299-1317.

12   Cronin, T., Raffelsberger, W., Lee-Rivera, I., Jaillard, C., Niepon, M.L., Kinzel, B., Clerin, E., Petrosian, A., Picaud, S., Poch, O. *et al.* The disruption of the rod-derived cone viability gene leads to photoreceptor dysfunction and susceptibility to oxidative stress. *Cell Death Differ.*, **17**, 1199-1210.

13   Rattner, A. and Nathans, J. (2005) The genomic response to retinal disease and injury: evidence for endothelin signaling from photoreceptors to glia. *J. Neurosci.*, **25**, 4540-4549.

14   Muller, T., Concannon, C.G., Ward, M.W., Walsh, C.M., Tirniceriu, A.L., Tribl, F., Kogel, D., Prehn, J.H. and Egensperger, R. (2007) Modulation of gene expression and cytoskeletal dynamics by the amyloid precursor protein intracellular domain (AICD). *Mol. Biol. Cell*, **18**, 201-210.

15   Fridlich, R., Delalande, F., Jaillard, C., Lu, J., Poidevin, L., Cronin, T., Perrocheau, L., Millet-Puel, G., Niepon, M.L., Poch, O. *et al.* (2009) The thioredoxin-like protein rod-derived cone viability factor (RdCVFL) interacts with TAU and inhibits its phosphorylation in the retina. *Mol. Cell. Proteomics*, **8**, 1206-1218.

16   Funato, Y. and Miki, H. (2010) Redox regulation of Wnt signalling via nucleoredoxin. *Free Radic. Res.*, **44**, 379-388.

17   Schwartz Levey, M., Chikaraishi, D.M. and Kauer, J.S. (1991) Characterization of potential precursor populations in the mouse olfactory epithelium using immunocytochemistry and autoradiography. *J. Neurosci.*, **11**, 3556-3564.

18   Matulionis, D.H. (1975) Ultrastructural study of mouse olfactory epithelium following destruction by ZnSO4 and its subsequent regeneration. *Am. J. Anat.*, **142**, 67-89.

19   Enwere, E., Shingo, T., Gregg, C., Fujikawa, H., Ohta, S. and Weiss, S. (2004) Aging results in reduced epidermal growth factor receptor signaling, diminished olfactory neurogenesis, and deficits in fine olfactory discrimination. *J. Neurosci.*, **24**, 8354-8365.

20   Mackay-Sim, A. and Beard, M.D. (1987) Hypothyroidism disrupts neural development in the olfactory epithelium of adult mice. *Brain Res.*, **433**, 190-198.

21   Newman, M.P., Feron, F. and Mackay-Sim, A. (2000) Growth factor regulation of neurogenesis in adult olfactory epithelium. *Neuroscience*, **99**, 343-350.

22   Pekkari, K., Avila-Carino, J., Gurunath, R., Bengtsson, A., Scheynius, A. and Holmgren, A. (2003) Truncated thioredoxin (Trx80) exerts unique mitogenic cytokine effects via a mechanism independent of thiol oxido-reductase activity. *FEBS Lett*, **539**, 143-148.

23   Arner, E.S. and Holmgren, A. (2000) Physiological functions of thioredoxin and thioredoxin reductase. *Eur. J. Biochem.*, **267**, 6102-6109.

24   Gao, J., Cheon, K., Nusinowitz, S., Liu, Q., Bei, D., Atkins, K., Azimi, A., Daiger, S.P., Farber, D.B., Heckenlively, J.R. *et al.* (2002) Progressive photoreceptor degeneration, outer segment dysplasia, and rhodopsin mislocalization in mice with targeted disruption of the retinitis pigmentosa-1 (Rp1) gene. *Proc. Natl. Acad. Sci. U S A*, **99**, 5698-5703.

25   Nishimura, D.Y., Fath, M., Mullins, R.F., Searby, C., Andrews, M., Davis, R., Andorf, J.L., Mykytyn, K., Swiderski, R.E., Yang, B. *et al.* (2004) Bbs2-null mice have neurosensory deficits, a defect in social dominance, and retinopathy associated with mislocalization of rhodopsin. *Proc. Natl. Acad. Sci. U S A*, **101**, 16588-16593.

26   Kim, J.C., Badano, J.L., Sibold, S., Esmail, M.A., Hill, J., Hoskins, B.E., Leitch, C.C., Venner, K., Ansley, S.J., Ross, A.J. *et al.* (2004) The Bardet-Biedl protein BBS4 targets cargo to the pericentriolar region and is required for microtubule anchoring and cell cycle progression. *Nat. Genet.*, **36**, 462-470.

27   Liu, X., Udovichenko, I.P., Brown, S.D., Steel, K.P. and Williams, D.S. (1999) Myosin VIIa participates in opsin transport through the photoreceptor cilium. *J. Neurosci.*, **19**, 6267-6274.

28   Kulaga, H.M., Leitch, C.C., Eichers, E.R., Badano, J.L., Lesemann, A., Hoskins, B.E., Lupski, J.R., Beales, P.L., Reed, R.R. and Katsanis, N. (2004) Loss of BBS proteins causes anosmia in humans and defects in olfactory cilia structure and function in the mouse. *Nat. Genet.*, **36**, 994-998.

29   Berndt, C., Lillig, C.H. and Holmgren, A. (2008) Thioredoxins and glutaredoxins as facilitators of protein folding. *Biochim. Biophy.s Acta.*, **1783**, 641-650.

30   Dulac, C. and Axel, R. (1995) A novel family of genes encoding putative pheromone receptors in mammals. *Cell*, **83**, 195-206.

31   Schwenk, F., Baron, U. and Rajewsky, K. (1995) A cre-transgenic mouse strain for the ubiquitous deletion of loxP-flanked gene segments including deletion in germ cells. *Nucleic Acids Res.*, **23**, 5080-5081.

32   Raffelsberger, W., Krause, Y., Moulinier, L., Kieffer, D., Morand, A.L., Brino, L. and Poch, O. (2008) RReportGenerator: automatic reports from routine statistical analysis using R. *Bioinformatics*, **24**, 276-278.

33   Ploner, A., Calza, S., Gusnanto, A. and Pawitan, Y. (2006) Multidimensional local false discovery rate for microarray studies. *Bioinformatics*, **22**, 556-565.

34   Limberis, M.P., Vandenberghe, L.H., Zhang, L., Pickles, R.J. and Wilson, J.M. (2009) Transduction efficiencies of novel AAV vectors in mouse airway epithelium in vivo and human ciliated airway epithelium in vitro. *Mol. Ther.*, **17**, 294-301.

35   Vandenberghe, L.H., Breous, E., Nam, H.J., Gao, G., Xiao, R., Sandhu, A., Johnston, J., Debyser, Z., Agbandje-McKenna, M. and Wilson, J.M. (2009) Naturally occurring singleton residues in AAV capsid impact vector performance and illustrate structural constraints. *Gene Ther.*, **16**, 1416-1428.

36   Gao, G.P., Alvira, M.R., Wang, L., Calcedo, R., Johnston, J. and Wilson, J.M. (2002) Novel adeno-associated viruses from rhesus monkeys as vectors for human gene therapy. *Proc. Natl. Acad. Sci. U S A*, **99**, 11854-11859.

37   Glisin, V., Crkvenjakov, R. and Byus, C. (1974) Ribonucleic acid isolated by cesium chloride centrifugation. *Biochemistry*, **13**, 2633-2637.

38   Reichman, S., Kalathur, R.K., Lambard, S., Ait-Ali, N., Yang, Y., Lardenois, A., Ripp, R., Poch, O., Zack, D.J., Sahel, J.A. *et al.* (2009) The homeobox gene CHX10/VSX2 regulates RdCVF promoter activity in the inner retina. *Hum. Mol. Genet.*, **19**, 250-261.

39   Slotnick, B. and Restrepo, D. (2005) Olfactometry with mice. *Curr. Protoc. Neurosci.*, **Chapter 8**, Unit 8 20.

40   Feron, F., Mackay-Sim, A., Andrieu, J.L., Matthaei, K.I., Holley, A. and Sicard, G. (1999) Stress induces neurogenesis in non-neuronal cell cultures of adult olfactory epithelium. *Neuroscience*, **88**, 571-583.

Legends to figures

Figure 1. *Nxnl2* targeting strategy. (**A**) Schema showing the wild-type (WT) *Nxnl2* allele, the targeted *Nxnl2* locus after homologous recombination and removal of the neomycin selection cassette after Cre mediated loxP recombination and deletion of *Nxnl2* exon1. X: XbaI. Dotted box: Southern probe. P1, P2, P3, P4: primer used for PCR genotyping. P1: 5'-TCCTATATGCTGGTTTCCGTC-3'; P2: 5'-TGATCAAGGAGCCTAGCTAAGG-3'; P3: 5'-TCGATTAGAGGTAGAAGAACCC-3' and P4: 5'-AGCTCCGTGTAGAAGTCGC-3'. (**B**) Southern hybridization with DNA from ES cells after excision of the neomycin selection cassette. DNA was digested with restriction enzyme XbaI. Hybridization was performed with a ^{32}P labelled *Nxnl2* probe. (**C**) PCR analysis was performed on DNA isolated from tail of wild-type, heterozygous and homozygous mice for the exon1 *Nxnl2* null allele.

Figure 2. Cone degeneration and dysfunction at 10 months in *Nxnl2-/- mice*. (**A**) Photopic ERG tracing from wild-type and *Nxnl2*-/- at 2 and 10 months of age. (**B**) Summarized photopic ERG data from 10 months of age mice (n = 10). (**C**) Photopic ERG from *Nxnl2*-/- mice retina treated at 6 months of age with AAV-GFP, AAV-RdCVF2 or untreated. AAV-RdCVF2 delivery to the retina prevents the loss of cone function observed at 10 months of age in the animal treated with AAV-GFP. (**D**) Number of cones was evaluated by counting PNA positive cells at 10 months of age. (**E**) Immunohistochemistry using PNA labeling and S-Opsin antibody on *Nxnl2*+/+ and *Nxnl2*-/- flat mounted retina. In *Nxnl2*-/- retina, the presence of cones labeled with PNA without expression of S-opsin is indicated with an arrow (Scale bar: 5 μm). (**F**) Immunohistochemistry using PNA labeling and M-Opsin antibody on *Nxnl2*+/+ and *Nxnl2*-/- cross sections in ventral part of retina. Scale bar : 20 μm.

Figure 3. Impaired rod function at 10 months in *Nxnl*2-/- mice. (**A**) Scotopic ERG tracing from wild-type and *Nxnl*2-/- at 10 months of age. (**B**) Summarized scotopic ERG data from 10 months of age (n = 10). (**C**) Spidergram showing ONL thickness in *Nxnl*2-/- and control mice at 8 months of age (n = 6). (**D**) Thinning of *Nxnl*2-/- and control ONL mice at 3, 8 and 18 months (n = 6).

Figure 4. RdCVF2 is essential to maintenance of outer segment length. (**A-C**) Ultrastructure of the outer retina in WT, *Nxnl1*-/- and *Nxnl2*-/- mice at 12 months of age. The transmission electron microscopy images show the stacked outer segments of the outer nuclear layer. Scale bar : 2 µm. (**D**) and (**E**) Scanning electron microscopy on *Nxnl*2+/+ and *Nxnl2*-/- retina at 12 months of age showed outer segment morphology. (**F**) Photoreceptor sensory cilium (PSC) complex was purified and stained with Rho4d2 and RPGRIP antibodies. (**G**) Outer segments from *Nxnl*2-/- and control mice at 10 months of age were stained with Rho4D2 antibody. (**H**) Length of outer segments was evaluated from *Nxnl*2-/- and control mice at 3 and 10 months of age (n = 3). Scale bars represent 5 µm. (**I**) Outer segments from control and *Nxnl*2-/- mouse retina were dissected using laser capture microdissection. Dissected outer segments and whole retina were immunoblotted with rhodopsin and actin antibodies. Quantification was evaluated using Image J software. (**J**) Representative fluorescence patterns in cryosections 3 months after subretinal injection with AAV2/8-GFP. ONL, outer nuclear layer. Scale bar represents 20 µm. (**K**) Length of outer segments of *Nxnl*2-/- mice treated with AAV2/8RdCVF2L.

Figure 5. Signaling pathways in *Nxnl*2-/- retina. (**A**) Immunolabeling of cryosections from control and *Nxnl*2-/- mice at 18 months of age with Glial Fibrillary Acidic Protein (GFAP, green) antibody. (**B**) Distribution of phosphorylated TAU (AT8) and TAU (Tau5) in 10 months mouse retina. Immunostaining of control and Nxnl2-/- was carried out using AT8 and

Tau5 antibodies. GC, ganglion cells; INL, inner nuclear layer; ONL, outer nuclear layer. (**C**) Western blotting on retinal lysates from control and Nxnl2-/- mice using beta catenin antibody. (**D**) Relative expression based on the microarray data of a selection of the target genes identified by false discovery rate method in the *Nxnl*1+/+, *Nxnl*1-/- *Nxnl*2+/+ and *Nxnl*2-/- retina.

Scale bar represents 50 µm.

Figure 6. Expression of both *Nxnl2* mRNAs by olfactory neurons. (**A, B**) *In situ* hybridization on olfactory epithelium sections with a digoxigenin-labeled RdCVF2 and RdCVF2L antisens riboprobes. The specificity of staining was shown with the sense probes (**C, D**). (**E**) Quantification of RdCVF2 and RdCVF2L mRNA 6 days post bulbectomy (OBX).

Figure 7. Olfactory discrimination performances of *Nxnl2*-/- mice decrease with age. (**A**) Go/No-go procedure in the olfactometer. (**B**) Mean percentage of correct responses in each block of two days (D1, D2) of training (n = 7-10 mice/group). S+ was (+)-Carvone and S- was (-)-Carvone. 50% represents chance level (dashed line) and 85% represents performance criterion (dotted line). (**C**) Mean percentage of correct responses for each training block of the seven days (D1 to D7) of training. Mice were trained to discriminate between (+)-Carvone (S+) and a mixture of (+)-Carvone and (-)-Carvone (S-). The concentration of (-)-Carvone in the S- mixture was reduced each day from 2×10^{-4} to 5×10^{-5}, 2×10^{-5}, 1.5×10^{-5}, 10^{-5}, 10^{-6} and 10^{-8}M. Thus, (-)-Carvone successively represented 20%, 5%, 2%, 1.5%, 1%, 0.1% and 0.001% of the mixture. (**D**) Mean percentage of correct responses for all training blocks for each day of the seven days (D1 to D7). $*p < 0.005$, $**p = 0.01$, $***p < 0.001$ (n = 7-10). Error bars indicate the SEM. 2 M-WT: wild-type two-month-old mice (*n* = 9), 2 M-KO: *Nxnl*2-/- two-

month-old mice ($n = 9$), 12 M-WT: wild-type twelve-month-old mice (n = 10), 12 M-KO: *Nxnl2*-/- twelve-month-old mice (n = 7).
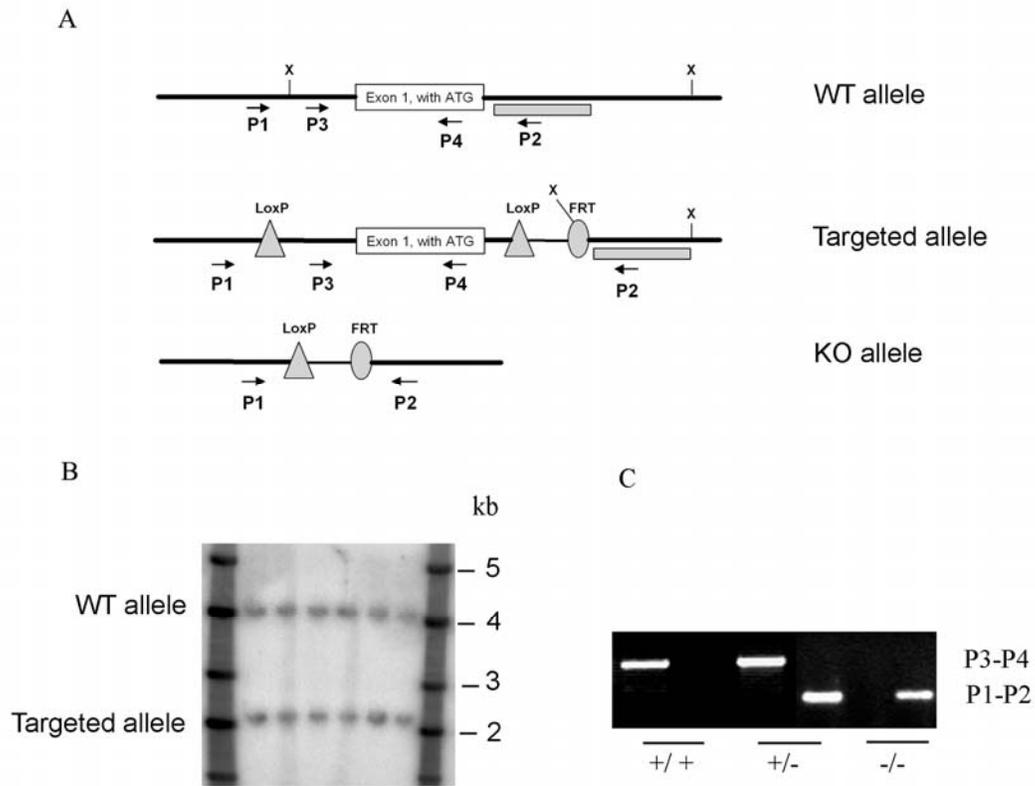
Figure 8. RdCVF2 promotes survival of adult olfactory sensory neurons (OSNs) *in vitro*. Survival of OSNs in culture by adding respectively media from COS-1 cells transfected with empty vector pcDNA3, pcDNA-RdCVF2, pcDNA-RdCVF2L (**A, B, C**) and GST, GST-RdCVF2, GST-RdCVF2L (**D**).
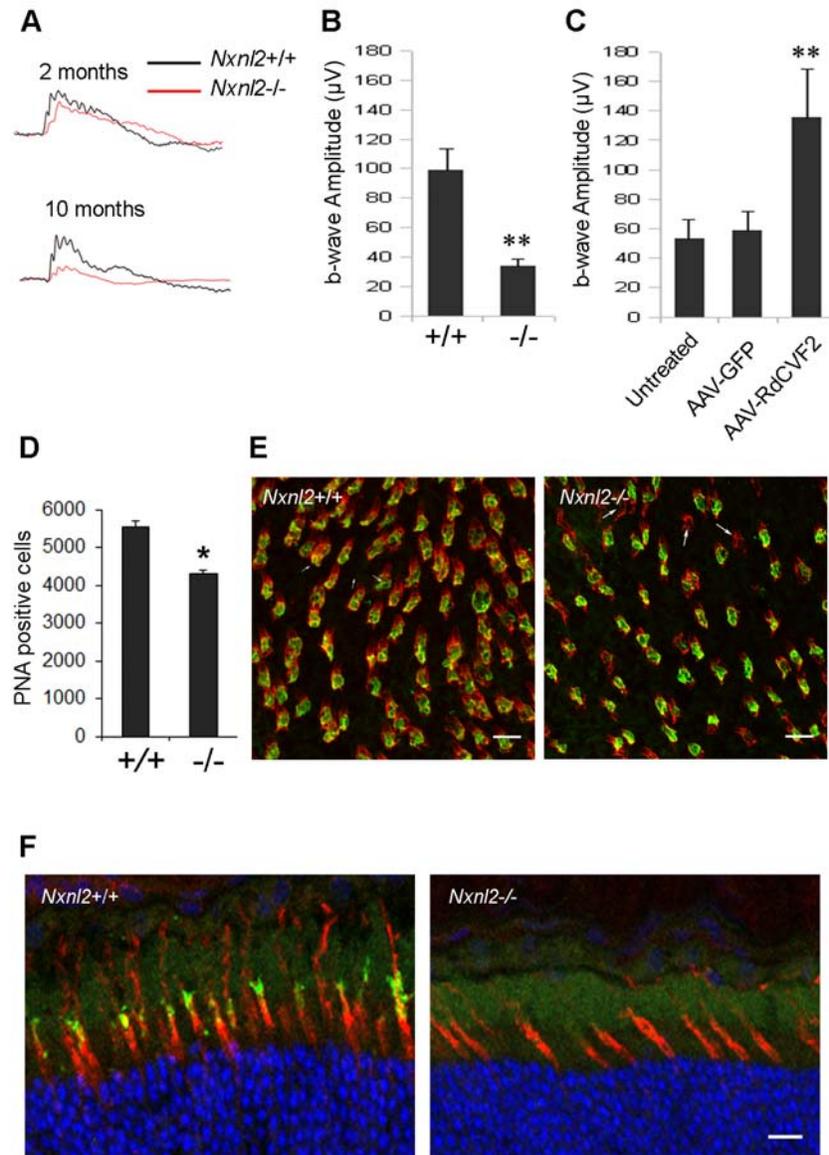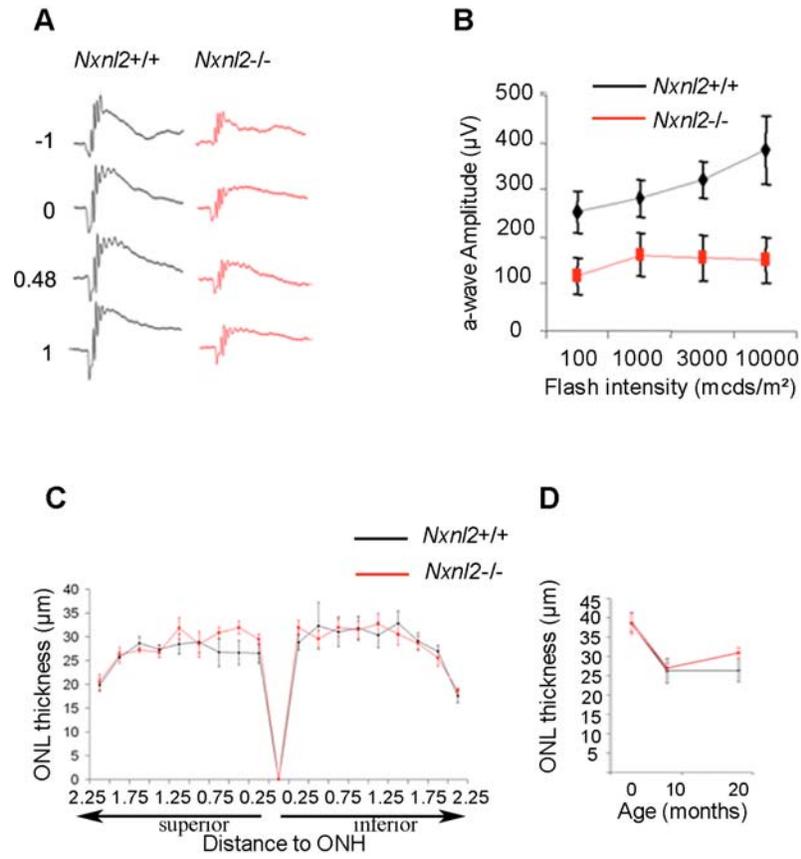
Abbrevations

Nxnl: Nucleoredoxin-like

RdCVF: Rod derived cone viability factor
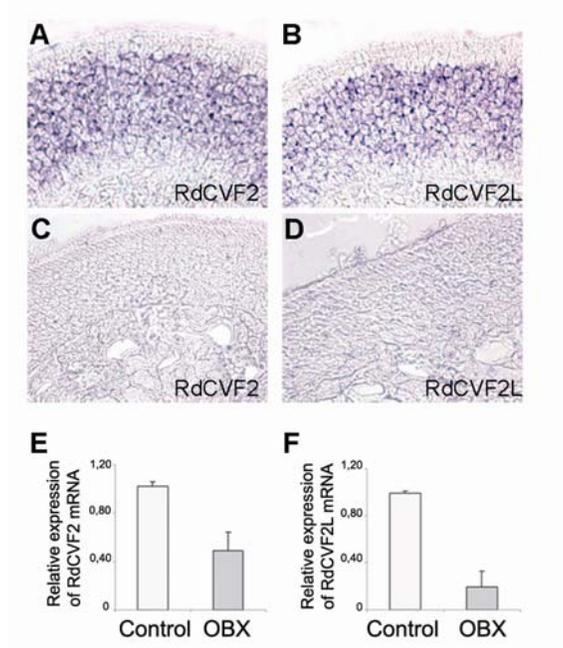
A

B

C

Fig. 1

Fig. 2
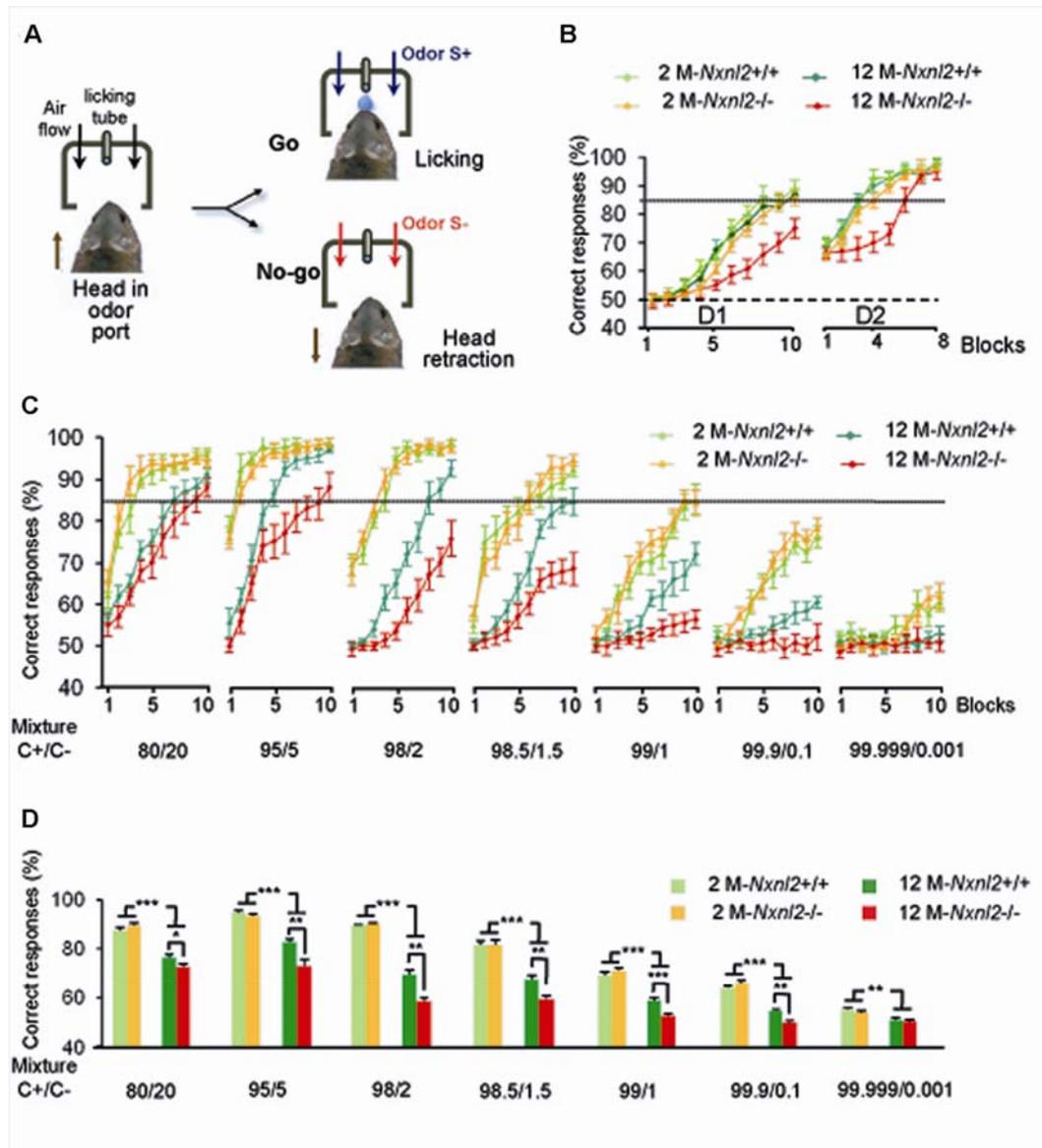
Fig. 3

Fig. 4

Fig. 5

Fig. 6

Fig. 7

Fig. 8